ARTICLES

Elastic scattering of N-, L-, and S-type polarized 794 MeV protons from an ND_3 target polarized in the S-L plane

E. Gülmez, D. L. Adams,* S. Beedoe, M. Bleszynski, J. Bystricky,† V. Ghazikhanian, G. Igo, T. Jaroszewicz, and A. G. Ling‡
University of California, Los Angeles, California 90024

M. Nasser
King Fahd University of Petroleum and Minerals, Box 175, Dhahran 31261, Saudi Arabia

M. W. McNaughton and S. Penttilä
Los Alamos National Laboratory, Los Alamos, New Mexico 87545

G. Glass
Texas A&M University, College Station, Texas 77843

G. Kahrimanis, W. F. Kielhorn, K. H. McNaughton, P. J. Riley, S. Sen,§ and D. Wolf
University of Texas, Austin, Texas 78712
(Received 13 May 1991)

23 p-d elastic scattering spin observables, most of them in linear combinations of two observables, were measured at 794 MeV over a range of four-momentum transfer t from -0.257 to -0.630 $(\mathrm{GeV}/c)^2$. By changing the beam polarization between S, N, and L type and by alternating the target vector polarization between negative and positive, six independent combinations of beam and target polarization were obtained. The target was dynamically polarized deuterated ammonia. An average target polarization of 30% was achieved. Transverse polarization components of the scattered protons (S and N type) were measured directly by using a polarimeter. The longitudinal polarization component (L type) was measured after precessing it to N type. Typical uncertainties for two-spin coefficients were 0.02 and for three-spin coefficients 0.1–0.2. The data are compared with the theoretical predictions calculated by fitting the previously available data to a relativistic multiple-scattering model with derivative couplings. Although relativistic impulse approximation calculations do not predict the data well, they are also included in the comparisons.

PACS number(s): 25.40.Cm, 24.70.+s, 25.10.+s, 29.25.Pj

I. INTRODUCTION

It has been argued that the measurement of p-d elastic scattering in the angular interval where single and double scattering are thought to predominate provides a unique testing ground for various N-N models. Studying p-d elastic scattering could lead to a better understanding of the processes contributing to nucleon-nucleus scattering. This is particularly true at larger angles where off-mass-shell effects and three-body interactions become important. Thus it is important to increase the p-d elastic-scattering data and to improve the statistical accuracy at larger angles.

At 800 MeV (nominal proton-beam energy), considerable progress has been made toward obtaining a complete set of measurements (at least 23 observables) with sufficiently small error bars over the single- and double-scattering regions to provide a stringent test of theoretical models. Measurement of more spin observables than the required minimum (23) have been at least partially completed. Among them $C_{N0,00}$ and $C_{0N,00}$ (S, N, and L in the Ann Arbor convention [1]; see Sec. III for the definitions) have been measured several times [2–8] Rahbar *et al.* [3], Sun *et al.* [9], and Igo *et al.* [10] measured the spin observables $C_{S0,L0}$, $C_{L0,S0}$, $C_{S0,S0}$, $C_{L0,L0}$, and $C_{N0,N0}$. Haji-Saied *et al.* [5] measured the tensor spin observables $C_{0\,NN,00}$ and $C_{0\,SS,00}$ using a 1600-MeV deute-

*Present address: Rice University, Houston, TX 77251.
†Permanent address: DPhPE, CEN Saclay, 91191 Gif-sur-Yvette CEDEX, France.
‡Present address: Los Alamos National Laboratory, Los Alamos, NM 87545.
§Present address: Physics Department, Thomas More College, Crestview Hills, KY 41017.

ron beam, which yields the same center-of-mass energy as an 800-MeV proton. In a recent experiment at Saclay (Ghazikhanian *et al.* [7,8]), these two tensor spin observables were measured in addition to $C_{N\,NN,00}$, $C_{N\,SS,00}$, $C_{0\,SL,00}$, $C_{N\,SL,00}$, $C_{L\,SN,00}$, $C_{LS,00}$, $C_{0S,S0}$, $C_{NS,S0}$, $C_{0N,N0}$, $C_{NN,00}$, $C_{NN,N0}$, $C_{0\,SS,N0}$ $C_{N\,SS,N0}$, $C_{0\,NN,N0}$, $C_{N\,NN,N0}$, $C_{0\,NS,S0}$, and $C_{N\,NS,S0}$. This experiment also utilized a 1600-MeV deuteron beam. Recently published works [6,11] report more spin-observable measurements from The High Resolution Spectrometer (HRS) Facility at Los Alamos, including $C_{SL,00}$, $C_{LL,00}$, $C_{N\,LL,00}$, $C_{0L,S0}$, $C_{0L,L0}$, $C_{SL,N0}$, $C_{NL,S0}$, $C_{NL,L0}$, $C_{LL,N0}$, $C_{NN,00}$, $C_{0N,N0}$, $C_{NN,N0}$, $C_{SN,S0}$, $C_{SN,L0}$, $C_{LN,S0}$, and $C_{LN,L0}$. The unpolarized elastic-scattering differential cross section has been measured by Irom *et al.* [4], Winkelmann *et al.* [2], and, most recently, by Gülmez *et al.* [12].

The number of spin observables listed above exceeds the minimum number of observables necessary to determine the elastic-scattering amplitudes. Since the deuteron has spin 1, the p-d elastic scattering could be represented by 12 complex amplitudes or 23 independent real quantities (spin observables) with an overall phase factor. On the other hand, an examination of the data sets mentioned above would reveal that some data sets do not extend to large four-momentum-transfer regions [$-t > 0.3$–0.4 (GeV/c)^2], which is important for the investigation of off-mass-shell effects. Also, some of the observables have large errors, causing relatively small weighting factors in any kind of fitting scheme. The data set of this work improves the coverage in a significant portion of the region where double scattering is believed to be predominant [$-t > 0.3$–0.4 (GeV/c)^2].

II. EXPERIMENTAL METHOD

The data reported here were taken at the EPB-N experimental area at the Los Alamos Clinton P. Anderson Meson Physics Facility (LAMPF experiment 818). The experiment was designed for the purpose of obtaining data mostly in the double-scattering region to complement previous measurements. All three orientations of beam polarization, S, N, and L (in the Ann Arbor convention [1]), were used. The target polarization was in the S-L plane with a small N component. The configuration of the polarized target magnet was the reason for such a complicated target polarization, instead of a target polarization completely in one direction.

The protons and coincident deuterons were detected in a two-arm detector system (Fig. 1). The data were taken at four different angular settings of the proton arm (p arm). Weighted averages of the scattering angle for each angle setting were 21.60°, 24.25°, 28.35°, and 32.61° [or $-t = 0.282$, 0.348, 0.471, and 0.592 (GeV/c)^2]. For analyzing-power measurements, each of these angle settings was further divided into three bins, covering a four-momentum-transfer region from 0.257 to 0.630 (GeV/c)^2. Each angular setting covered about 3° in scattering and azimuthal angles.

A. Polarized proton beam

A polarized 798-MeV proton beam was produced by a Lamb-shift ion source (the effective beam energy at the center of the target was 794 MeV due to the energy losses in the target and surrounding material). Three orthogonal orientations of the proton polarization vector in the scattering frame of reference were obtained by a combination of solenoid and bending magnets upstream of the target. Incoming spins were precessed such that the additional precession due to the fields of the final bending magnet between the beam-line polarimeters and the polarized target magnet would produce the desired orientation of the polarization vector at the scattering plane. Polarization of the beam particles were monitored during the experiment by a system of two beam-line polarimeters with a bending magnet between them. The bend angle for 798-MeV protons was 29°. Combining two sets of N and S components of the beam polarization measured by the two beam-line polarimeters and taking into account the magnetic field of the bending magnet and the polarized target magnet, the beam polarization vector at the target was obtained. Typical polarization along the desired direction (S, N, or L) in the scattering reference frame was 70–75 % with a 10–20 % component in the other directions. The magnitude of the beam polarization was also measured by comparing the beam intensities of polarized and quenched states. These two methods consistently agreed throughout the experiment. The direction of the beam polarization vector was reversed every 2 min to reduce the systematic errors by canceling some of the instrumental effects. Beam intensity was monitored with an ion chamber upstream of the target and also with the beam-line polarimeters. Typically, the average beam intensity was kept below 5–6 pA because of the wire-chamber limitations.

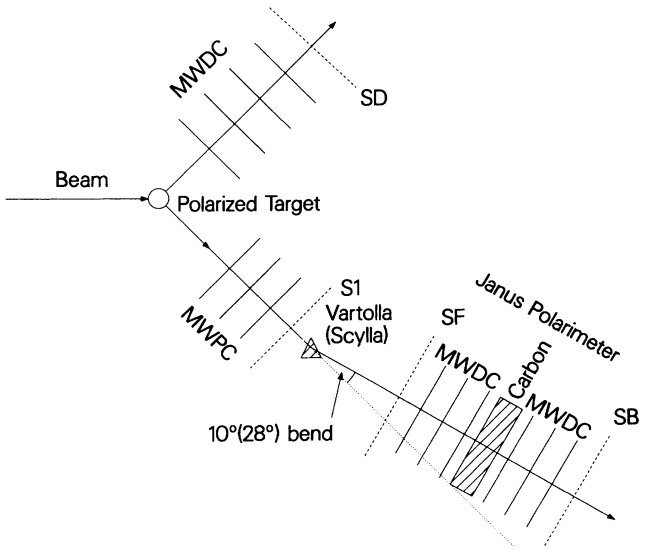

FIG. 1. Schematic layout of the experiment to measure spin observables in p-d elastic scattering. The spectrometer bend angle was about 28° upward in the first phase using the SCYLLA magnet. A 10° bend toward the beam line in the horizontal plane was obtained using the VARTOLLA magnet in the second phase of the experiment.

B. Polarized deuteron target

Deuterated (99%) ammonia (ND_3) was selected as the target material because its deuteron content is greater than that of commonly used alcohols. Furthermore, the radiation resistivity of ND_3 material is better than that of any alcohol-type target material [13]. The ND_3 material was in the form of small crystals (average size, 2 mm). In Ref. [14], the preparation of the material is described in detail.

The ND_3 material was placed in a 1.8-cm-diameter and 3-cm-long perforated cylindrical Teflon cell. The areal thickness of the target was 1.56×10^{-4} deuteron/mb. The packing fraction was 0.6. The cell was in the mixing chamber of the dilution refrigerator operated just below the $^3He/^4He$ phase boundary. The cylindrical axis of the target cell was parallel to the 2.5-T field of the Hera split-coil (Helmholtz-type) superconducting magnet. The magnet/cryostat system together with pumps and gas cart were rotated about the target center on the floor to accommodate the requirement of the scattering angles. The target magnetic field and temperature were maintained at 2.5 T and 0.45 K, respectively.

Two different methods were used to analyze the target polarization data. These were the thermal equilibrium (TE) method and fitting the deuteron magnetic resonance (DMR) absorption signal.

The TE method is based on the fact that the vector component of the polarization is proportional to the area of the absorption part of the DMR signal. In principle, the DMR signal can be determined by first measuring the base-line signal off resonance, then making a measurement on resonance. The DMR signal is extracted by subtracting the base-line signal. In our case, the simple subtraction of the base line did not eliminate the base-line component totally [see Fig. 2(a)]. It was found to be necessary to fit the residual base line with a third-order polynomial. This suggests that the residual base line is mainly due to noise in the system, since there was no correlation between adjacent third-order polynomial fits. Thermal calibrations were done several times during the experiment. While collecting scattering data, a polarization value was calculated with a tentative TE calibration every 8 sec and the enhanced DMR signals were recorded every 5 min [15].

An independent measurement of the target polarization was to fit the DMR signal. This is possible because the deuteron quadrupole moment interacts with the molecular electric field gradient and this interaction splits the Zeeman states. The vector and tensor polarizations of the deuteron target could be extracted from the measured DMR spectrum by fitting to a theoretical curve [Fig. 2(b)]. Details of this fitting procedure are given in Refs. [14] and [16]. The advantage of this second method is that it is not dependent on the TE measurements. An underlying assumption is that an equilibrium spin temperature has been established in the deuteron spin ensemble (Ref. [14]). This assumption of equal spin temperature (EST) provides the following useful relationship between the vector and tensor polarizations:

$$P_T=2-\sqrt{4-3P_V^2}\ , \tag{1}$$

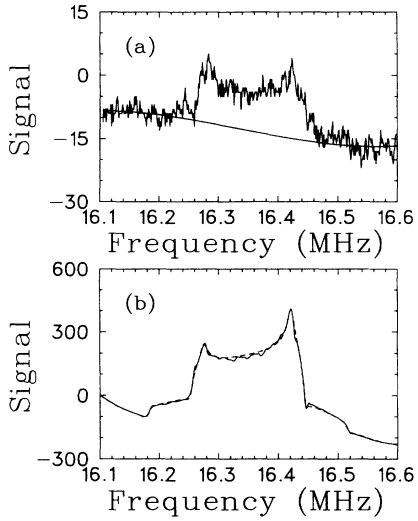

FIG. 2. Deuteron magnetic resonance (DMR) signals for (a) the target material at thermal equilibrium (TE) and (b) the dynamically enhanced deuteron polarization signal. The DMR signal in (a) is the signal measured at the resonance minus the signal (base line) measured out of the resonance. The smooth curve in (a) is the third-order polynomial representing the random background mentioned in the text. The coefficients of the third-order polynomial were obtained by fitting the wings of this difference signal. The polarization value obtained from the Boltzmann statistics for the signal shown is 0.051% for 1.016 K and 2.5 T. The dashed curve in part (b) is the theoretical DMR signal obtained by fitting the actual DMR signal (solid curve). The vector polarization value for this DMR signal is 34% (the fitting gives 35.7%).

where P_T and P_V are the tensor and vector polarizations in the cylindrically symmetric target reference frame, respectively. It is important to note that the EST assumption is essential in treating the DMR fitting method and the TE method as being independent. Otherwise both must be used to determine the values of P_V and P_T. In our data analysis, EST was assumed to be established. Thus Eq. (1) was used to calculate P_T.

The polarization of the target changed rapidly when the polarization direction was reversed or the polarization was enhanced from the unpolarized state. The EST assumption, hence the relationship between the vector and tensor polarizations [Eq. (1)], was not valid during these rapid changes in the polarization [14]. The tensor polarization during this kind of transition period could still be determined by using both the DMR fitting method and the TE method. The latter gives the vector polarization and then, using this vector polarization, the tensor polarization could be extracted from the line-shape fitting. Changes in the polarization direction were infrequent. Runs with polarization significantly lower than the average polarization were not included in the analysis. Figure 3 displays the vector polarization of the target as a function of time during the experiment. The polarization values shown in Fig. 3 are those derived by the TE method. These were corrected by a factor (1.02

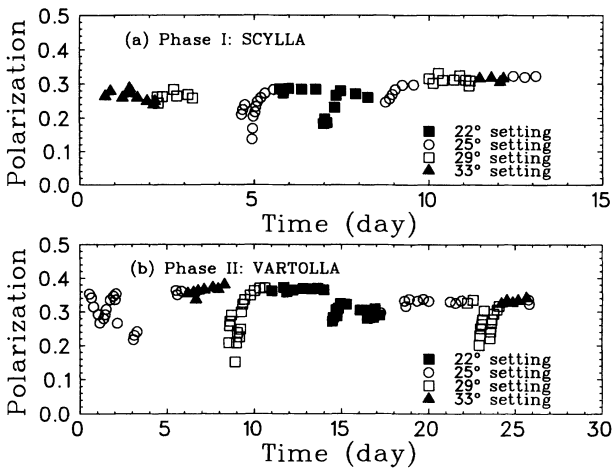

FIG. 3. The target and vector polarizations as a function of time is displayed (a) for the first and (b) for the second phase of the experiment. The angular settings of the spectrometer are indicated in the figures. The statistical errors are smaller than the size of the points. Systematic uncertainties of the order of 5% are not included in the figures.

or 1.05 depending on the case) obtained by comparing the results of the second method with the corresponding values obtained using the TE method for a sample of signals. The average of these independent measurements was used to obtain the correction factor.

C. Detectors

The determination of the trajectories of the scattered proton and deuteron was crucial in selecting out p-d elastic-scattering events from the much larger number of p-p quasielastic events produced. The proton arm (Fig. 1) consisted of two sets of chambers, one upstream of the momentum analyzer magnet (SCYLLA or VARTOLLA) and another, downstream of it. Three multiwire proportional chambers (MWPC's) determined the trajectory of the scattered protons upstream of the momentum analyzer magnet. Typical combined efficiency of these MWPC's was ~50%. Three multiwire delay-line drift chambers (MWDLDC's or MWDC's) downstream of the analyzer magnet determined the trajectory of the protons deflected by the magnet. The analyzer magnet SCYLLA (VARTOLLA) was set for a nominal vertical (horizontal) bend angle of approximately 28° (10°).

During the first phase of the experiment, the beam polarization was of the N type. The target polarization was mainly in the S-L plane and had comparable components in both S and L directions. Parity conservation excludes an N-type component of polarization for the outgoing proton in three-spin observables in this set of circumstances. This was the reason for bending the protons upward by 28°, i.e., precessing the L component of the polarization of the elastically scattered protons through 90° to N type, which made it possible to measure the longitudinal component of the polarization vector. All six of the MWDLDC's, including those discussed above, were part of the JANUS polarimeter [17]. Using carbon blocks (total thickness, 25.4 cm) in the middle of the polarimeter as the analyzer, the S and N components of the polarization vector (in the polarimeter reference frame) of the scattered protons could be measured.

There were four MWDLDC's in the deuteron arm (d arm) to determine the trajectory of the particles scattered to the left (see Fig. 1). The split-coil polarizing magnet was oriented, for each scattering-angle setting, such that the particles scattered to the left in coincidence with the particles detected in the p arm would pass through a separation (22 cm) between the two coils. Utilization of the four chambers to obtain three sets of coordinates of the recoil particle's trajectory resulted in high overall chamber efficiency in the d arm (~80%). The combined chamber efficiency for the proton and deuteron arms was about 40%.

A coincidence between two scintillator planes (SF, SB) and a single ended scintillator (S1) (Fig. 1) provided the p-arm trigger. A coincidence signal produced with an appropriate delay between the p-arm trigger and the trigger signal from the detector SD in the d-arm was used as the master trigger for the data-acquisition system.

III. FORMALISM

The spin observables $C_{ij,kl}$ are defined by the expression

$$C_{ij,kl}=\frac{\mathrm{tr}(\hat{F}\hat{\sigma}_i\hat{J}_j\hat{F}^\dagger\hat{\sigma}_k\hat{J}_l)}{\mathrm{tr}(\hat{F}\hat{F}^\dagger)}\ , \tag{2}$$

where i,j,k,l are the polarization directions of the proton and deuteron before and after the scattering, respectively. The spin observables $C_{ij,kl}$ may not necessarily be the same as those defined by the Ann Arbor convention [1]. In this experiment, the polarization of the outgoing deuteron is not measured, thus the notation is reduced to $C_{ij,k}$. The deuteron in the target may have polarization j of the vector and tensor type. The quantities $\hat{F}$, $\hat{\sigma}$, and $\hat{J}$ are the elastic-scattering matrix, the spin-$\frac{1}{2}$, and the spin-1 matrices, respectively. These coefficients can be further simplified when k does not enter and will be called, A_{ij}, analyzing powers.

The polarized cross section Y can be formulated as

$$Y=\mathrm{tr}(\hat{F}\rho_{\mathrm{in}}\hat{F}^\dagger)\ , \tag{3}$$

where ρ_{in} is the combined density matrix and

$$\rho_{\mathrm{in}}=\rho_p\rho_d\ . \tag{4}$$

The density matrices ρ_p and ρ_d are

$$\rho_p=\tfrac{1}{2}(1+p_S\sigma_S+p_N\sigma_N+p_L\sigma_L) \tag{5}$$

and

$$\begin{aligned}\rho_d=\tfrac{1}{3}\{1+\tfrac{3}{2}P_V(\alpha J_S+\beta J_N+\gamma J_L)+\tfrac{1}{2}P_T[(\alpha^2-\gamma^2)J_{SS}\\ +\tfrac{1}{2}P_T[(\alpha^2-\gamma^2)J_{SS}\\ +2\alpha\beta J_{SN}+2\alpha\gamma J_{SL}+(\beta^2-\gamma^2)J_{NN}\\ +2\beta\gamma J_{NL}]\}\ ,\end{aligned} \tag{6}$$

where

$$\alpha=\sin\theta_t\cos\phi\ ,$$
$$\beta=-\sin\theta_t\sin\phi\ , \tag{7}$$
$$\gamma=\cos\theta_t\ .$$

θ_t is the angle between the target polarization direction (parallel with the magnetic field direction of the target, which is the z direction in the laboratory frame of reference) and the beam direction (laboratory frame of reference). P_V and P_T are the vector and tensor components of the deuteron polarization and ϕ is the azimuthal angle between the scattering plane and the target plane. the scattering plane is defined by the incoming and outgoing proton momentum vectors and the target plane is defined by the incoming proton momentum and the target polarization vector. In the scattering reference frame, the z direction (L) points downstream along the beam direction, the y direction (N) points down, and the x direction points to the right of the beam direction.

A. Two-spin observables

A useful quantity is the experimental asymmetry:

$$\epsilon=\frac{Y(\mathbf{p})-Y(-\mathbf{p})}{Y(\mathbf{p})+Y(-\mathbf{p})}\ , \tag{8}$$

where Y is a measured yield with beam polarization $\mathbf{p}$. ϵ may be expressed as

$$\epsilon=p_S[U_1+\tfrac{3}{2}P_V U_2]+\tfrac{3}{2}p_L P_V U_3+p_N\{A_{N0}+\tfrac{3}{2}P_V\beta A_{NN}+\tfrac{1}{2}P_T[(\alpha^2-\gamma^2)A_{N\,SS}+2\alpha\gamma U_4+(\beta^2-\gamma^2)A_{N\,NN}]\}$$
$$\times\{1+\tfrac{3}{2}P_V\beta A_{0N}+\tfrac{1}{2}P_T[(\alpha^2-\gamma^2)A_{0\,SS}+2\alpha\gamma A_{0\,SL}+(\beta^2-\gamma^2)A_{0\,NN}]\}^{-1}\ , \tag{9}$$

where

$$U_1=A_{S0},\quad U_2=\alpha A_{SS}+\gamma A_{SL}\ ,$$
$$U_3=\alpha A_{LS}+\gamma A_{LL},\quad U_4=A_{N\,SL}\ . \tag{10}$$

Equation (9) is valid if small terms proportional to $P_T\beta$ are neglected. The asymmetry A_{S0} must be zero due to parity conservation. It was left in the expression to check for systematic errors. By fitting the six independent measurements (alluded to earlier in this paper) of the asymmetry ϵ to the above expression, it was possible to extract the combinations of spin observables U_1 to U_4.

B. Three-spin observables

Three-spin observables required the measurement of the components of the polarization vector of the scattered proton, using the JANUS polarimeter. Twenty-four quantities were measured, including S- and N-type components (in the polarimeter reference frame) of the polarization of the outgoing protons for normal and reverse cycles of the beam polarization for all combinations of beam and target polarization orientations. The polarization components of the scattered protons can be formulated in terms of the scattering matrix $\hat{F}$ and the density matrix $\rho_{\rm in}$ as

$$P'_X=\frac{\mathrm{tr}(\hat{F}\rho_{\rm in}\hat{F}^\dagger\sigma_X)}{\mathrm{tr}(\hat{F}\rho_{\rm in}\hat{F}^\dagger)}\ , \tag{11}$$

where X is any one of the polarization directions: S, N, or L. However, these polarization components refer to the scattering reference frame, whereas the measured polarization components P''_N and P''_S are in the reference frame of the JANUS polarimeter. In order to fit the measured values, the above expressions have to be transformed into the JANUS polarimeter reference frame, taking into account the precessions in the field of the polarizing magnet and bending magnet. The final expressions for S''- and N''- type spins are

$$P''_S=f(\mathbf{p})\{\tfrac{3}{2}P_V[R_{SS}U_1+R_{SL}U_2+p_S R_{SN}U_3+p_N(R_{SS}U_4+R_{SL}U_5)+p_L R_{SN}U_6]$$
$$+p_S(R_{SS}U_7+R_{SL}U_8)+p_N R_{SN}U_9+p_L(R_{SS}U_{10}+R_{SL}U_{11})+R_{SN}U_{12}\}\ , \tag{12}$$
$$P''_N=f(\mathbf{p})\{\tfrac{3}{2}P_V[R_{NS}U_1+R_{NL}U_2+p_S R_{NN}U_3+p_N(R_{NS}U_4+R_{NL}U_5)+p_L R_{NN}U_6]$$
$$+p_S(R_{NS}U_7+R_{NL}U_8)+p_N R_{NN}U_9+p_L(R_{NS}U_{10}+R_{NL}U_{11})+R_{NN}U_{12}\}\ , \tag{13}$$

where $f(\mathbf{p})$ is $Y_0/6Y$ for normal or reversed states of the beam polarization. The quantities R_{IJ} are the components of the precession and rotation matrix, $P''_X=R_{XY}P'_Y$. Y_0 and Y are given as

$$Y_0=\mathrm{tr}(\hat{F}\hat{F}^\dagger)\ , \tag{14}$$
$$Y=\mathrm{tr}(\hat{F}\rho_{\rm in}\hat{F}^\dagger)$$
$$=\frac{Y_0}{6}+\tfrac{3}{2}P_V\beta A_{0N}+\frac{P_T}{2}[(\alpha^2-\gamma^2)A_{0\,SS}+2\alpha\gamma A_{0\,SL}+(\beta^2-\gamma^2)A_{0\,NN}]$$
$$+\tfrac{3}{2}p_S P_V(\alpha A_{SS}+\gamma A_{SL})+p_N\left[A_{N0}+\tfrac{3}{2}P_V\beta A_{NN}+\frac{P_T}{2}[(\alpha^2-\gamma^2)A_{N\,SS}+2\alpha\gamma A_{N\,SL}+(\beta^2-\gamma^2)A_{N\,NN}]\right]$$
$$+\tfrac{3}{2}p_L P_V(\alpha A_{LS}+\gamma A_{LL})\ , \tag{15}$$

and the quantities U_n are defined as

$$
\begin{aligned}
&U_1=\alpha C_{0S,S}+\gamma C_{0L,S},\quad U_2=\alpha C_{0S,L}+\gamma C_{0L,L}\ ,\\
&U_3=\alpha C_{SS,N}+\gamma C_{SL,N},\quad U_4=\alpha C_{NS,S}+\gamma C_{NL,S}\ ,\\
&U_5=\alpha C_{NS,L}+\gamma C_{NL,L},\quad U_6=\alpha C_{LS,N}+\gamma C_{LL,N}\ ,\\
&U_7=C_{S0,S}+X_{SA,S}\approx C_{S0,S},\quad U_8=C_{S0,L}+X_{SA,L}\approx C_{S0,L}\ ,\\
&U_9=C_{N0,N}+X_{NA,N}\approx C_{N0,N},\quad U_{10}=C_{L0,S}+X_{LA,S}\approx C_{L0,S}\ ,\\
&U_{11}=C_{L0,L}+X_{LA,L}\approx C_{L0,L},\quad U_{12}=C_{00,N}+X_{0A,N}\approx C_{00,N}\ ,
\end{aligned}
\tag{16}
$$

where

$$
X_{iA,j}=\tfrac{3}{2}\bar{P}_V\beta C_{iN,j}+\frac{\bar{P}_T}{2}[(\alpha^2-\gamma^2)C_{i\,SS,j}+2\alpha\gamma C_{i\,SL,j}+(\beta^2-\gamma^2)C_{i\,NN,j}]\ . \tag{17}
$$

$\bar{P}_V$ and $\bar{P}_T$ are averaged quantities over the whole experiment (0.30 and 0.069, respectively). In addition to dropping terms proportional to $P_T\beta$, some terms proportional to P_T or β were also neglected. This is justified because of the dominating statistical uncertainty. P_T, β, and $P_T\beta$ are always less than 0.1 and typical uncertainties in the three-spin observables reported here are 0.1–0.2. A detailed account of the formalism in more general terms is given in Ref. [8].

IV. ANALYSIS OF THE SCATTERING DATA

The feasibility of the experiment and the soundness of the method to identify and separate the p-d elastic-scattering events from a large background of p-p quasielastic-scattering events was established in a test run. The test run was performed under similar conditions except that an unpolarized deuteron target (CD_2) was used. During the test run, a momentum analyzing magnet was located at the end of the d arm. It was found not to be necessary in the procedure adopted to identify the valid deuterons and thus was not included in the final experimental setup.

A VAX750 computer with an associated CAMAC data-acquisition system was employed. Most p-p elastic-scattering events were rejected by a combination of hardware and software tests before the data were written on tape. The hardware filtering was achieved by using the p-arm trigger signal (coincidence of S1·SF·SB) to define the master-trigger timing and by adjusting the relative timing of the p-arm and d-arm (SD) trigger signals with an appropriate width for the d-arm trigger signal. Any event that had a relative time of flight between the two arms outside a specific interval was rejected. This hardware cut did not eliminate many p-p quasielastic events, because the time interval was fairly wide in order to include all p-d elastic events. Tighter limits were set on the time-of-flight spectrum through the microbranch driver (MBD) processor in the data-acquisition system. An MBD test rejected a significant portion of the p-p quasielastic-scattering events. A small sample of the total events were written to the data tapes regardless of the MBD test results to monitor possible asymmetries introduced by this test.

More restrictive gates were set on several histograms accumulated during the replay. These include the relative time of flight, the energy loss in the d-arm scintillator (SD), the difference between the scattering angle measured by the p-arm chambers and the same angle calculated from the deuteron scattering angle ($\Delta\theta$), the coplanarity, the tracebacks to the target position from the chambers in each arm, and the requirements for a valid chamber event. Somewhat similar tests were used during data acquisition to monitor the experiment.

As seen in Fig. 4, the relative times of flight for protons and deuterons in the d arm were resolved fairly well. In fact the gates on the histogram of this relative time of flight eliminated almost all of the p-p quasielastic events except those in the p-p quasielastic tail inside the gate and under the p-d elastic peak, which were eliminated with the other tests.

The pulse heights of the signals coming from the SD scintillator in the d arm were proportional to the energy

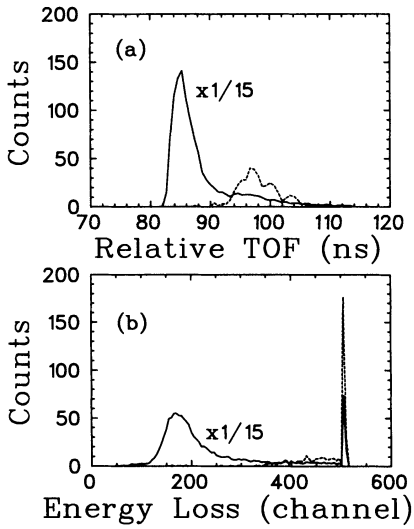

FIG. 4. (a) The distribution of the events as a function of the relative time difference between the two arms (TOF). (b) The distribution of the energy losses of the particles passing through the SD scintillator. Events selected as being good p-d elastic scattering events are also presented (dashed curves). In (a) and (b), the solid curve is scaled down by a factor of 15. For all the distributions displayed here only those events that were recorded regardless of the MBD test results were used.

loss (which is proportional to the velocity) of the particles in this arm. Since the velocities of the proton and deuteron differ by approximately a factor of 2, there was good separation of p-d elastic and p-p quasielastic events [Fig. 4(b)]. Although there was a large overlap of events rejected by the energy loss and time of flight, some of the events not rejected by the time-of-flight test were eliminated by the energy-loss tests.

After the time-of-flight and energy-loss tests, there were not many p-p quasielastic-scattering events remaining. The exceptions were the events that were both in the time-of-flight gate and in the Landau tail of the proton distribution in the energy-loss histogram, the random events, and the events not originating from the target. Random events and the remaining p-p quasielastic events were eliminated by the kinematical quantities $\Delta\theta$ and coplanarity (Fig. 5). $\Delta\theta$ is the difference between the measured scattering angle in the proton arm and this angle calculated from the measured angle of the particle in the deuteron arm through p-d kinematics. The coplanarity test requires that both scattered particles be in the same plane (the scattering plane). The angles measured in both arms were first corrected for the deflection caused by the field of the polarizing magnet. Events originating from points other than the target and also some of the random events were rejected by selecting the events whose trajectories trace back to the target position. Target trace-

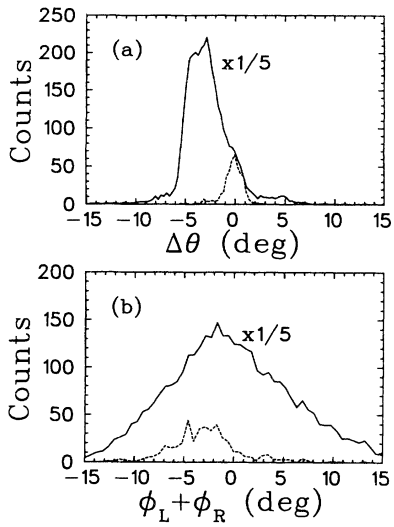

FIG. 5. (a) The quantity $\Delta\theta$ (defined in text) for all events (solid curve) scaled down by a factor of 5 and for the good p-d elastic-scattering events (dashed curve). (b) The coplanarity distribution $\sum\phi$ for all events (solid curve) scaled down by a factor of 5 and for the good p-d elastic-scattering events (dashed curve). The events used are those for which the MBD test was skipped.

TABLE I. Analyzing powers.

θ_{target} (deg)	θ_{lab} (deg)	ϕ (deg)	$-t$ (GeV/c)^2	$\alpha A_{SS}+\gamma A_{SL}$ [a]	$\alpha A_{LS}+\gamma A_{LL}$ [a]	$A_{N\,SL}$ [a]
22	20.55	−9.00	0.257	−0.135 ±0.019±0.008	−0.088 ±0.021±0.005	−0.521 ±0.708±0.258
22	21.37	−8.65	0.276	−0.161 ±0.019±0.004	−0.098 ±0.018±0.008	−1.243 ±0.501±0.274
22	22.31	−8.27	0.299	−0.171 ±0.017±0.004	−0.120 ±0.016±0.009	−0.833 ±0.746±0.439
25	23.40	−6.79	0.326	−0.197 ±0.023±0.005	−0.124 ±0.020±0.016	−0.169 ±0.262±0.545
25	24.20	−6.39	0.347	−0.237 ±0.024±0.005	−0.069 ±0.020±0.016	0.598 ±0.233±0.455
25	25.00	−6.27	0.369	−0.263 ±0.024±0.009	−0.038 ±0.020±0.014	0.814 ±0.470±0.150
29	27.36	−6.30	0.433	−0.189 ±0.017±0.004	0.015 ±0.015±0.004	0.378 ±0.198±0.159
29	28.64	−6.02	0.471	−0.149 ±0.020±0.005	0.042 ±0.017±0.005	0.334 ±0.234±0.134
29	29.68	−6.33	0.503	−0.185 ±0.022±0.005	0.038 ±0.019±0.008	0.361 ±0.312±0.115
33	31.55	−5.33	0.559	−0.147 ±0.020±0.005	0.050 ±0.015±0.008	0.832 ±0.207±0.125
33	32.66	−5.23	0.594	−0.142 ±0.020±0.005	0.052 ±0.016±0.004	0.666 ±0.199±0.129
33	33.82	−5.16	0.630	−0.136 ±0.019±0.004	0.070 ±0.015±0.008	0.634 ±0.251±0.137

[a] α and β are defined in Eq. (7). The uncertainties listed in each column are the statistical and systematical uncertainties. The uncertainties reported for the previous measurements and the overall systematic uncertainty of the target polarization measurement are the main contributors to the systematic uncertainty listed in each column. The systematic uncertainties in the beam ($\sim$1% [19]) and scattered particle's ($\sim$2% [20]) polarization measurements are not included (see text).

TABLE II. Spin transfer coefficients.

θ_{target} (deg)	θ_{lab} (deg)	ϕ (deg)	$-t$ (GeV/c)^2	$\alpha C_{0S,S}+\gamma C_{0L,S}$[a]	$\alpha C_{0S,L}+\gamma C_{0L,L}$[a]	$\alpha C_{SS,N}+\gamma C_{SL,N}$[a]	$\alpha C_{NS,S}+\gamma C_{NL,S}$[a]	$\alpha C_{NS,L}+\gamma C_{NL,L}$[a]	$\alpha C_{LS,N}+\gamma C_{LL,N}$[a]
22	21.60	−8.77	0.282	−0.178 ±0.079±0.009	−0.173 ±0.093±0.017	0.142 ±0.141±0.021	0.046 ±0.179±0.023	0.013 ±0.155±0.012	−0.251 ±0.146±0.021
25	24.25	−6.45	0.348	−0.276 ±0.067±0.008	0.014 ±0.068±0.014	0.002 ±0.181±0.013	−0.356 ±0.136±0.020	0.216 ±0.106±0.010	−0.071 ±0.178±0.023
29	28.35	−6.06	0.462	−0.380 ±0.065±0.008	0.091 ±0.070±0.008	−0.161 ±0.147±0.012	−0.121 ±0.134±0.012	0.270 ±0.108±0.010	−0.033 ±0.143±0.012
33	32.61	−5.26	0.592	−0.286 ±0.061±0.008	0.042 ±0.068±0.014	0.014 ±0.149±0.021	−0.082 ±0.134±0.020	−0.010 ±0.107±0.010	−0.041 ±0.128±0.011

[a]α and β are defined in Eq. (7). The uncertainties listed in each column are the statistical and systematical uncertainties. The uncertainties reported for the previous measurements and the overall systematic uncertainty of the target polarization measurement are the main contributors to the systematic uncertainty listed in each column. The systematic uncertainties in the beam (~1% [19]) and scattered particle's (~2% [20]) polarization measurements are not included (see text).

TABLE III. Spin rotation coefficients.

θ_{target} (deg)	θ_{lab} (deg)	ϕ (deg)	$-t$ (GeV/c)^2	$C_{S0,S}+X_{SA,S}$[a]	$C_{S0,L}+X_{SA,L}$[a]	$C_{N0,N}+X_{NA,N}$[a]	$C_{L0,S}+X_{LA,S}$[a]	$C_{L0,L}+X_{LA,L}$[a]	$C_{00,N}+X_{0A,N}$[a]
22	21.60	−8.77	0.282	0.797 ±0.146±0.021	−0.217 ±0.219±0.026	1.149 ±0.146±0.012	0.476 ±0.130±0.011	0.970 ±0.160±0.022	0.184 ±0.034±0.006
25	24.25	−6.45	0.348	0.892 ±0.156±0.013	−0.633 ±0.237±0.015	0.934 ±0.108±0.010	0.352 ±0.118±0.019	0.632 ±0.125±0.011	0.100 ±0.032±0.006
29	28.35	−6.06	0.462	0.566 ±0.112±0.018	−0.239 ±0.178±0.023	0.978 ±0.097±0.017	0.599 ±0.105±0.010	0.350 ±0.121±0.011	0.164 ±0.030±0.005
33	32.61	−5.26	0.592	0.488 ±0.128±0.011	−0.355 ±0.210±0.025	1.024 ±0.087±0.009	0.524 ±0.088±0.009	0.413 ±0.100±0.010	0.314 ±0.029±0.005

[a]The quantity $X_{iA,j}$ is defined in Eq. (17). The uncertainties listed in each column are the statistical and systematical uncertainties. The uncertainties reported for the previous measurements and the overall systematic uncertainty of the target polarization measurement are the main contributors to the systematic uncertainty listed in each column. The systematic uncertainties in the beam (~1% [19]) and scattered particle's (~2% [20]) polarization measurements are not included (see text).

backs were calculated from all three chamber systems, *d*-arm MWDLDC's, MWPC's, and the front JANUS chambers. However, the tracebacks from the MWPC's were not used in these tests because of the low efficiencies of these chambers (a valid trajectory through each chamber system that supplied any histogram used in the tests discussed above was a prerequisite). On the other hand, the MWPC's were used to calibrate the *p*-arm geometry and monitor the actual bend in the bending magnet. The measured bend angle from the MWPC's was not used because of the low efficiency. However, this limitation was overcome using the tracebacks from the JANUS front chambers, which included the bend-angle information indirectly. A trajectory tracking back to the target position meant that the bend angle, and hence the momentum of the proton, was correct.

After all these tests, a 2–10% background still remained. The correction for the remaining background events was obtained by placing gates on both sides of the *p-d* elastic-scattering peak in the $\Delta\theta$ histogram and accumulating background events that passed all the other tests for *p-d* elastic scattering and these background gates in the $\Delta\theta$ histogram. Then the yield for each angle bin was corrected by subtracting the background yields from the total yield. About 5% of the total events written to tape were *p-d* elastic-scattering events.

In addition to these tests for selecting the *p-d* elastic events, additional tests were required to make sure that the instrumental asymmetries were minimal in the JANUS polarimeter [17,18]. Any event whose alternate $(\phi+\pi)$ trajectory missed the back scintillator plane (SB) was rejected for both analyzing-power and spin-transfer coefficient measurements. An alternate trajectory is obtained by rotating the trajectory of the proton after the carbon analyzer by 180° around the trajectory before the scattering, i.e., the *z* direction for the carbon scattering. It was shown that this reduces instrumental asymmetries inherent in the system since SB was part of the master trigger [18]. Additional tests, used only for spin-transfer parameter measurements, were tests to define the acceptance of the polarimeter for the scattering in the carbon and to eliminate the protons that underwent multiple scatterings and forward scattering in the carbon. The analyzing power of carbon at forward scattering angles is too small to be useful. These additional tests lowered the useful fraction of events to 0.5–1.0% of the total events recorded on tape.

Yields for each beam and target spin combination states were also corrected for live time (typically 70–80%), overall chamber efficiencies, beam intensity, and MBD cuts. Typical asymmetries introduced by the MBD cuts were between 1% and 8%, which were corrected for during the data analysis. The statistical uncertainties in live time, beam intensity, chamber efficiencies, and MBD cuts were included in the statistical uncertainties reported in Tables I–III.

V. RESULTS AND CONCLUSION

Two kinds of spin observables were extracted from the data. One set of spin observables was obtained by fitting the six asymmetries from each case of beam and target polarization combinations by Eq. (9). Four standard spin observables or combinations of standard spin observables were variables in this fitting. The results of these fits at each angular setting are displayed in Fig. 6 and tabulated in Table I [A_{S0} is presented in Fig. 6(b) only]. Even though A_{S0} should be zero according to parity conservation it was still treated as a nonzero quantity in the fits as a way of checking the systematic problems in the whole method, experiment, analysis, and final fitting. The data points [Fig. 6(b)] are consistent with zero. Measuring A_{S0} as zero does not completely rule out all possible problems but it gives more confidence in the results. In fitting the asymmetries by Eq. (9), some of the previously measured analyzing-power values were used in the asymmetry expression [Eq. (9)]. These were A_{N0} from Winkelmann *et al.* [2] and A_{NN}, A_{NSS}, A_{NNN}, A_{0N}, A_{0SS}, A_{0SL}, and A_{0NN} from Ghazikhanian *et al.* [7,8]. The uncertainties in these previously measured quantities and the overall uncertainty in the target polarization (~5%) are included in the systematical uncertainties reported in Tables I–III. However, the systematical uncertainties in the beam polarization measurement [19] (~1%) and the scattered particle's polarization measurement [20] (~2%) are not included in the values given in Tables I–III. These should be added to the total uncertainty. The average χ^2 per degree of freedom, χ^2/D.F., was about 1.3.

The uncertainties in all other two-spin-observable

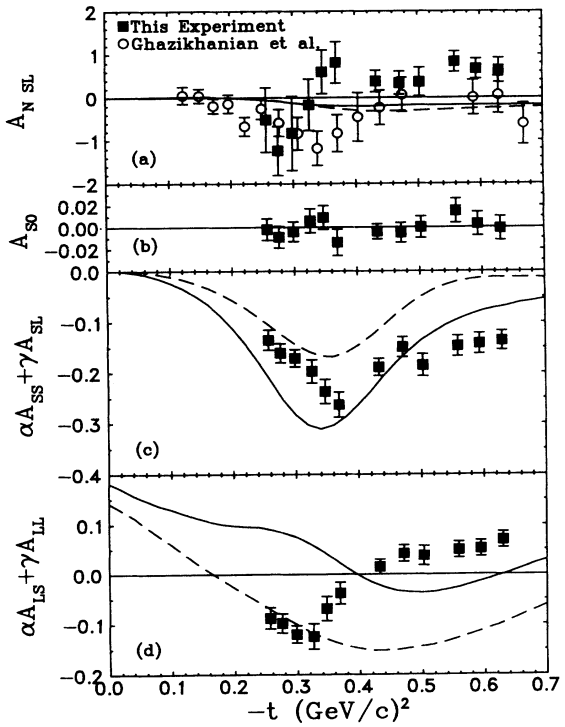

FIG. 6. Analyzing powers resulting from fitting the six asymmetries obtained from the experiment. The predictions obtained by using the RIA (dashed curve) and by using an interaction with derivative coupling (solid curve) are also shown.

combinations measured are small compared to the uncertainty of A_{NSL}. A_{NSL} is sensitive to the tensor polarization and to $\sin\phi$ (ϕ is the azimuthal angle between the target and the scattering reference frames as explained in Sec. III). The large uncertainty in A_{NSL} [Fig. 6(a)] arises because both of those are small. The average tensor polarization of the target was about 6.9% and sometimes as low as 4%. A comparison of the A_{NSL} measured by Ghazikhanian *et al.* [7,8] and the results obtained in this experiment [Fig. 6(a)] shows reasonable agreement between the two data sets except at three points around $-t \sim 0.35$. However, the large error bars prevent any definite conclusion one way or another. In fact, the target tensor polarization value for one of the N-type spin cases corresponding to these three data points was even smaller than the average value. Another complication that occurred during this low target polarization case was that the target polarization was slowly increasing, which means that the EST assumption used may not be valid. As expressed above, the tensor polarization was calculated with Eq. (1), which assumes that an EST has been established. If this equilibrium state does not exist, the tensor polarization cannot be calculated reliably from the vector polarization. Since the determination of A_{NSL} is very sensitive to the tensor polarization, any problems in that may effect the final results drastically.

The N- and S-type polarization components of the scattered proton measured by the JANUS polarimeter were fit to the expressions given in Eqs. (12) and (13) to give a second set of results. There were 24 measurements [two polarization components × three beam polarizations × two beam states (normal, reverse) × two target states (plus, minus)]. The fitting results were examined in two groups, the spin-transfer coefficients (Fig. 7) and the spin rotation parameters including the polarization (Fig. 8). Even though the spin rotation parameters and the polarization were measured in an earlier experiment, they were also extracted in our fitting. The uncertainties in the spin rotation parameters obtained in this measurement are much larger than those of the previously reported measurements. However, as seen in Fig. 8, the spin rotation parameters obtained in this experiment do not disagree with the previous measurements even though the spin rotation parameters extracted in this experiment include an additional small factor [$X_{iA,j}$'s in Eq. (15)] which seems to be negligible compared to the spin rotation parameters. In fact, the magnitude of this additional factor is smaller than the total uncertainty. For the sake of completeness, the values of the spin rotation parameters are also tabulated in addition to the spin-transfer coefficients. The average χ^2/D.F. for the fits to obtain these 12 coefficients was about 1.73.

Finally, the experimental results are compared with calculations based on multiple-scattering models. In this

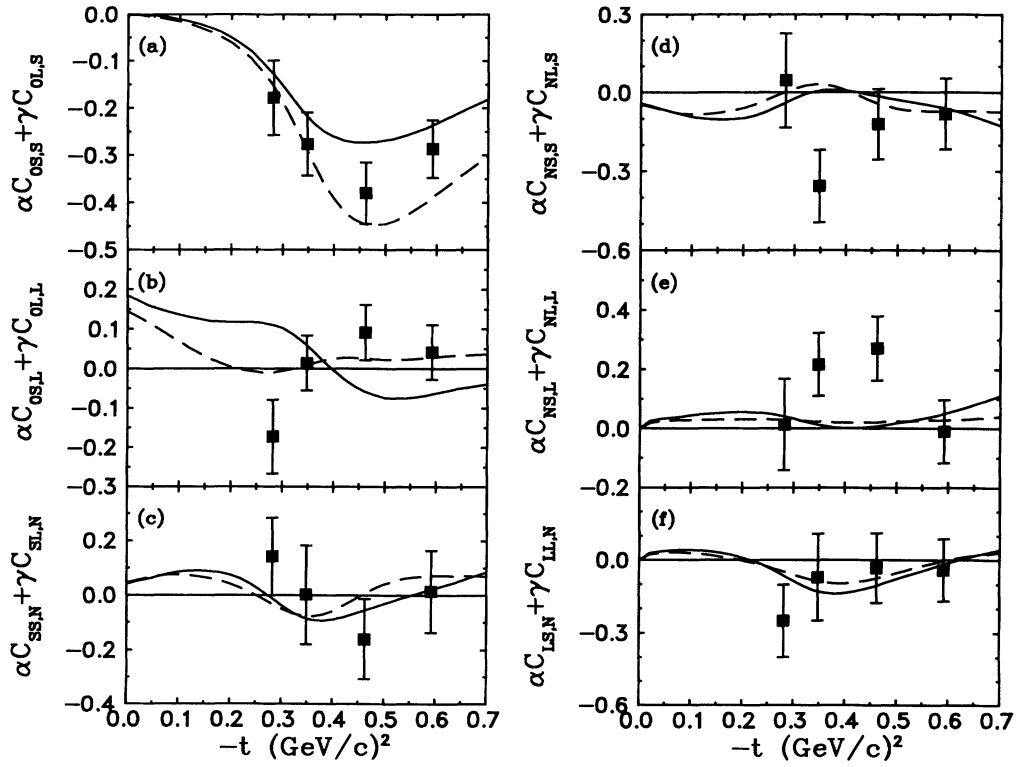

FIG. 7. Combinations of spin-transfer coefficients obtained by fitting the 24 polarization vector components (N and S components in the polarimeter reference frame) measured with the JANUS polarimeter. The predictions obtained by using the RIA (dashed curve) and by using an interaction with derivative coupling (solid curve) are also shown.

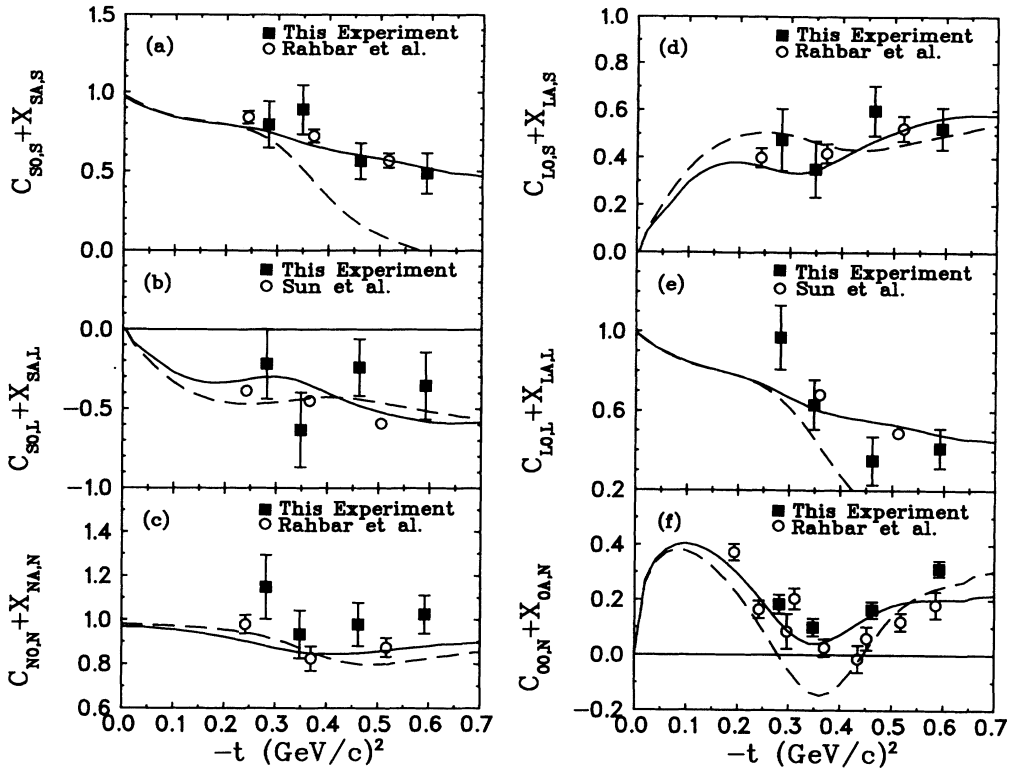

FIG. 8. Spin rotation coefficients obtained by fitting data from the 24 polarization vector components measured with the JANUS polarimeter. The predictions obtained by using the RIA (dashed curve) and by using an interaction with derivative coupling (solid curve) are shown. Data from Refs. [3] and [9] are also displayed.

approach the amplitude for p-d scattering is evaluated as a sum of single- and double-scattering terms, involving proton scattering off one and both target nucleons, respectively. The single-scattering contribution involves only the physical N-N scattering amplitude (known from partial-wave analysis), and the deuteron wave function, whose properties are also well established. The double-scattering term, however, requires additional information on the off-mass-shell behavior of the N-N amplitudes, related to the fact that the projectile nucleon propagates between the two scattering events. In this sense, the double-scattering amplitude is model dependent. In particular, the relativistic impulse approximation (RIA [21]) (which has been successful in describing polarized proton scattering on heavy- and medium-weight nuclei) assumes that relativistic N-N scattering amplitudes, both on *and* off mass shell, can be represented as combinations of the usual five Fermi covariants involving no momentum factors, and multiplied by invariant amplitudes depending only on the invariant energy and momentum transfers.

Significantly better agreement with the p-d scattering experiments can be obtained, however, by allowing for an additional off-mass-shell dependence of the N-N scattering amplitude. Physically, this dependence is expected to arise from the composite nature of nucleons [22], and from derivative meson-nucleon couplings [23]. The N-N scattering amplitude is then expressed as

$$F(p',p)=\sum_{a=S,V,T,A,P}\sum_{I=0,1}\left[1+\xi_a^I\frac{\not{p}'-M}{2M}\right]\times K_a P_I A_a^I(p',p)\times\left[1+\xi_a^I\frac{\not{p}-M}{2M}\right], \quad (18)$$

where p and p' are the initial and final projectile nucleon momenta, the A_a^I are invariant amplitudes (assumed to depend only on the energy and momentum-transfer invariants), and the P_I are isospin operators projecting on states of isospin I in the exchange (t) channel. The spin operators K_a, acting in the projectile- and target-nucleon spinor spaces, are the Fermi covariants: scalar (S), vector (V), tensor (T), axial (A), and pseudoscalar (P). This expression reduces to the standard representation of the physical N-N scattering amplitude on the mass shell. In general, nonzero coefficients ξ generate a nontrivial off-mass-shell dependence, which is expected to arise (in the sense of the low-energy derivative expansion) from derivative meson-nucleon couplings and from nucleon compositeness [23].

The coefficients ξ are treated as phenomenological parameters to be adjusted, in reasonable limits, to fit the experimental observables. Such phenomenological fits to all measured spin observables at 800 MeV, including the un-

polarized cross section, have been performed [12] (including the results of the current experiment which is in progress). This calculation employed the physical on-mass-shell amplitudes obtained from the recent solution SM89 to the N-N phase-shift analysis [24], and the deuteron wave functions based on the Reid soft-core potential [25]. The calculated observables were used to form the combinations that can be compared with quantities measured in this experiment.

The measured spin-observable combinations depend on the azimuthal angle ϕ and the polarized target angle θ_t, which was approximated as $\theta_{\rm lab}+0.55°$ to give better agreement with the average scattering angle for each setting. An empirical parametrization of the azimuthal angle as a function of the scattering angle was obtained, based on the facts that the magnetic field direction was roughly along the direction of the outgoing protons and the scattered deuterons were moving approximately perpendicular to the magnetic field. A least-squares fit of the azimuthal angles by the function derived from a simple magnetic field model gave

$$\sin\phi=\frac{0.079-0.0255/\cos\theta_{\rm lab}}{\sin\theta_{\rm lab}}\ , \tag{19}$$

where $\theta_{\rm lab}$ and ϕ are the scattering polar and azimuthal angles in the laboratory frame. Values for the azimuthal angle and polarized target angle for each bin are given in all the tables. The spin observables calculated with the values of the parameters listed above and combined in the way denoted by Eqs. (10), (16), and (19) are shown in Figs. 6, 7, and 8 as solid curves.

For comparison, results obtained with the RIA N-N off-mass-shell amplitudes [26] are displayed by dashed lines in Figs. 6, 7, and 8. As in the full multiple-scattering-model calculation, the SM89 partial-wave solution and the Reid soft-core deuteron wave function were used. It is apparent that the spin observables are not reproduced correctly by the RIA assumption. The disagreement between the RIA results and the spin observables becomes particularly pronounced at larger angles, where double scattering and associated off-mass-shell effects are significant. This is especially true for spin observables $C_{S0,S}$ and $C_{L0,L}$.

There is general agreement between the theoretical predictions displayed by the solid lines and the data. For spin observables whose magnitude are close to zero, such as $C_{SS,N}$ coupled with $C_{SL,N}$ and $C_{LS,N}$ coupled with $C_{LL,N}$, the predictions are also close to zero and agree with the data reasonably well within the error bars. It should be kept in mind that the derivative-coupling parameters ξ were obtained by a fit to all the available spin-observable data measured earlier [3,9], but *not* to the data of the present experiment. Therefore, there is, in general, a better agreement with the previously measured observables.

The results of the measurements presented here are expected to further constrain the phenomenological parameters ξ, and thus provide additional information on the off-mass-shell N-N amplitudes and on the dynamics of the three-nucleon system.

There are plans to reduce the experimental uncertainties, particularly in the case of the three-spin observables and to extend the measurement of the spin observables to larger angles. New experiments of this type are planned using a deuteron beam at Saclay with a scintillating fiber array instead of wire chambers for faster data acquisition.

ACKNOWLEDGMENTS

We wish to thank M. Begala for his help during the experiment, the staff of the polarized target section of LAMPF for their effort to keep the target polarization at a high level, and V. Armijo for his help in refurbishing some of the MWDLDC's. We also would like to thank Professor D. Crabb and the BATES accelerator staff for their help in the initial high-temperature irradiation of the ND_3 target material. This work was supported in part by the U.S. DOE.

[1] *Higher Energy Polarized Beams (Ann Arbor, 1977)*, Proceedings of the Workshop, edited by A. D. Krisch and A. J. Salthouse, AIP Conf. Proc. No. 42 (AIP, New York, 1978), p. 142.

[2] E. Winkelmann, P. R. Bevington, M. W. McNaughton, H. B. Willard, F. H. Cverna, E. P. Chamberlin, and N. S. P. King, Phys. Rev. C **21**, 2535 (1980).

[3] A. Rahbar, B. Aas, E. Bleszynski, M. Bleszynski, K. Ganezer, G. J. Igo, F. Irom, B. E. Bonner, O. van Dyck, M. W. McNaughton, J. B. Roberts, C. Hollas, R. D. Ransome, and P. J. Riley, Phys. Lett. B **194**, 338 (1987).

[4] F. Irom, G. J. Igo, J. B. McClelland, C. A. Whitten, Jr., and M. Bleszynski, Phys. Rev. C **28**, 2380 (1983).

[5] M. Haji-Saied, E. Bleszynski, M. Bleszynski, J. Carrol, G. J. Igo, T. Jaroszewicz, A. T. M. Wang, A. Sagle, J. B. McClelland, C. L. Morris, R. Klem, T. Joyce, Y. Makdishi, M. Marshak, B. Mossberg, E. A. Peterson, K. Ruddick, and J. Whittaker, Phys. Rev. C **36**, 2010 (1987).

[6] D. L. Adams, B. Aas, E. Bleszynski, M. Bleszynski, G. J. Igo, C. Newsom, Y. Ohashi, G. Pauletta, F. Sperisen, C. A. Whitten, Jr., H. Fujisawa, M. Gazzaly, S. J. Greene, K. Jones, J. B. McClelland, N. Tanaka, H. Hasai, K. Iwatani, S. Ishimoto, S. Isagawa, A. Masaike, A. Okihana, and S. Okumi, Nucl. Phys. **A480**, 530 (1988).

[7] V. Ghazikhanian, Ph.D. thesis, University of California, Los Angles, 1988.

[8] V. Ghazikhanian *et al.*, Phys. Rev. C **43**, 1532 (1991).

[9] Sun Tsu-hsun, B. E. Bonner, M. W. McNaughton, H. Ohnuma, O. B. van Dyck, G. S. Weston, B. Aas, E. Bleszynski, M. Bleszynski, G. J. Igo, D. J. Cremans, C. L. Hollas, K. H. McNaughton, P. J. Riley, R. F. Rodebaugh, S. Xu, and S. E. Turpin, Phys. Rev. C **31**, 515 (1985).

[10] G. Igo, M. Moshi, B. Aas, T. Jaroszewicz, C. Whitten, and K. Jones, in *High Energy Spin Physics,* Proceedings of the 9th International Symposium, Bonn, Federal Republic of Germany, 1990, edited by K. H. Althoff and W. Meyer (Springer-Verlag, Berlin, 1991), p. 505.

[11] G. Igo *et al.*, Phys. Rev. C **38**, 2777 (1988).

[12] E. Gülmez *et al.*, Bull. Am. Phys. Soc. **34**, 1140 (1989); E. Gülmez *et al.*, Phys. Rev. C **43**, 2067 (1991).

[13] R. Dostert, W. Havenith, O. Kaul, E. Kohlgarth, W. Meyer, E. Schilling, G. Sternal, W. Thiel, and K. H. Althoff, *Proceedings of the 4th International Workshop on Polarized Target Materials and Techniques,* Bad Honnef, Federal Republic of Germany, 1984, edited by W. Meyer (Physikalisches Institut Universität Bonn, Bonn, 1984), p. 33, and related papers in the same proceedings.

[14] W. F. Kielhorn, Ph. D. thesis, University of Texas at Austin, 1991.

[15] D. Hill and T. Kasprzyk, Argonne National Laboratory Report Series, No. ANL-HEP-PR-84-32.

[16] W. F. Kielhorn, E. Gülmez, J. J. Jarmer, and S. I. Penttilä, *Proceedings of the 8th International Symposium on High-Energy Spin Physics, Minnesota, 1988,* edited by Kenneth J. Heller, AIP Conf. Proc. No. 187 (AIP, New York, 1989), p. 1254.

[17] R. Ransome, S. J. Greene, C. L. Hollas, B. E. Bonner, M. W. McNaughton, C. L. Morris, and H. A. Thiessen, Nucl. Instrum. Methods **201**, 309 (1982).

[18] A. Rahbar, Ph.D. thesis, University of California, Los Angeles, 1982.

[19] M. W. McNaughton and E. P. Chamberlin, Phys. Rev. C **24**, 1778 (1981).

[20] M. W. McNaughton *et al.*, Phys. Rev. C **25**, 1967 (1984).

[21] R. J. Shepard, J. A. McNeil, and S. J. Wallace, Phys. Rev. Lett. **50**, 1443 (1983); B. C. Clark, S. Hama, L. R. Mercer, L. Ray, and B. D. Serot, *ibid.* **50**, 1644 (1983).

[22] E. Bleszynski, M. Bleszynski, and T. Jaroszewicz, Phys. Rev. Lett. **59**, 423 (1987).

[23] M. Bleszynski and T. Jaroszewicz, UCLA report, 1990 (unpublished).

[24] R. A. Arndt, L. D. Roper, R. A. Bryan, R. B. Clark, B. J. VerWest, and P. Signell, Phys. Rev. D **28**, 97 (1983); amplitude analysis code SAID, 1989 version.

[25] W. Reid, Ann. Phys. (N. Y.) **192**, 233 (1982).

[26] E. Bleszynski, M. Bleszynski, and T. Jaroszewicz, in *Intersections Between Particle and Nuclear Physics (Lake Louise, Canada),* Proceedings of the Second Conference, edited by D. F. Geesaman, AIP Conf. Proc. No. 150 (AIP, New York, 1986), p. 1208.